A comparison of Autonomous Techniques for Multispectral Image Analysis and Classification

Juan C. Valdiviezo-N.[a]*, Gonzalo Urcid[b], Carina Toxqui-Quitl[a], Alfonso Padilla-Vivanco[a]

[a]División de Ingenierías, Universidad Politécnica de Tulancingo, Tulancingo, Hidalgo, 43629, México;

[b]Coordinación de Óptica, INAOE, Tonantzintla, Puebla, 72000, México;

ABSTRACT

Multispectral imaging has given place to important applications related to classification and identification of objects from a scene. Because of multispectral instruments can be used to estimate the reflectance of materials in the scene, these techniques constitute fundamental tools for materials analysis and quality control. During the last years, a variety of algorithms has been developed to work with multispectral data, whose main purpose has been to perform the correct classification of the objects in the scene. The present study introduces a brief review of some classical as well as a novel technique that have been used for such purposes. The use of principal component analysis and K-means clustering techniques as important classification algorithms is here discussed. Moreover, a recent method based on the *min*-W and *max*-M lattice auto-associative memories, that was proposed for endmember determination in hyperspectral imagery, is introduced as a classification method. Besides a discussion of their mathematical foundation, we emphasize their main characteristics and the results achieved for two exemplar images conformed by objects similar in appearance, but spectrally different. The classification results state that the first components computed from principal component analysis can be used to highlight areas with different spectral characteristics. In addition, the use of lattice auto-associative memories provides good results for materials classification even in the cases where some spectral similarities appears in their spectral responses.

Keywords: autonomous techniques, image analysis, K-means, lattice associative memories, multispectral classification

1. INTRODUCTION

Multispectral imaging instruments have become an important tool for the analysis of objects in a scene due to their capability to derive spectral information about materials. Although these instruments were first used for Earth monitoring, during the last years they can be found as fundamental analysis tools in diverse areas. Current applications include: quality control,[12,15] color reproduction,[32] restoration of scripts in damaged manuscripts,[5,6,17] analysis of art works,[4,8] medicine,[34] among others. Multispectral devices register multiple images at different wavelength intervals from the ultraviolet, (UV), visible (VIS), or near infrared (NIR) ranges of the electromagnetic spectrum. The information acquired at each spectral band provides more information about materials than conventional cameras because the relative intensity of materials (*spectral radiance*) varies with wavelength. Moreover, appropriate techniques can be used to derive the spectral reflectance of materials comprising the scene under study.

During the last years, different algorithms have been proposed to perform the unsupervised classification of multiespectral data. The aim of classification is to identify regions in the scene with similar spectral characteristics. A commonly used method to quantify the spectral similarities between a reference spectrum and any other spectral pixel in the image is the *spectral angle mapper*, (SAM). Although this intensive method has been used for many applications,[7,21] it requires that the reference spectra should be known in advance. Because of the processing time required to analyze multiple images, analytical tools for dimensionality reduction, such as *principal component analysis* (PCA) or *partial least squares* (PLS) have been commonly used.[11,19] These algorithms have

* Corresponding author. Email: carlos.valdiviezo@upt.edu.mx, Phone:+52 775 755–8319

Applications of Digital Image Processing XXXV, edited by Andrew G. Tescher, Proc. of SPIE
Vol. 8499, 849920 · © 2012 SPIE · CCC code: 0277-786/12/$18 · doi: 10.1117/12.930289

been used to maximize the spectral differences within the image. Other common approaches contemplate the use of clustering techniques to group the data according to a predefined criterion; in this category we can mention classical techniques such as, K-means and fuzzy-C means.[2] Moreover, there exist a novel class of algorithms that has emerged from the context of hyperspectral data to give solution to the problem of autonomous identification of endmembers; in this context we can mention *pixel purity index* (PPI),[3] *vertex component analysis* (VCA),[18] and *lattice associative memories*.[25] Although these algorithms have been proposed to work with higher dimensional data, they can be properly modified to realize the classification of vectors with similar spectral curves.

The following manuscript provides a comparison of three autonomous techniques that are suitable for materials classification from multispectral imagery. We begin with a discussion of how principal component analysis can be used to maximize the spectral differences along the scene. Later, the mathematical treatment of K-means clustering and a technique for endmembers identification based on *lattice associative memories*, a novel development in lattice algebra, is presented. This manuscript is organized as follows: Section 2 introduces the mathematical basis of PCA and K-means clustering; Section 3 starts with a brief mathematical background on lattice algebra and then introduces the concept of lattice associative memories for pattern recognition. This Section concludes with a discussion of the use of both memories for image classification. Section 4 gives the classification results obtained by applying each technique to a pair of multispectral data sets. Concluding remarks and direction of future work to the research material presented in this paper are given in Section 5.

2. AUTONOMOUS TECHNIQUES FOR IMAGE CLASSIFICATION

The increasing use of multispectral sensors, where multiple bands of the same scene should be analyzed, has made necessary the development of improved techniques to work with the problem of classification of multidimensional data. In the following lines we present the mathematical treatment of two approaches commonly used in the literature, whose results have given solution to numerous problems.

2.1 Principal Component Analysis

The use of principal component analysis for image classification has been widely studied from different perspectives. The technique determines orthogonal linear combinations from a set of characteristics (spectral bands) that maximize the variance among them; this variations can be used to form a new set of images called *components*. Although the technique has been mainly studied for dimensionality reduction, it also may be used to combine components to form an enhanced image. Given an $M \times N$ multispectral image conformed by n spectral bands, we can represent the image as a set having $k = MN$ spectral pixels; i.e. $\mathbf{x}^\xi$ in $\mathbb{R}^n$ for $\xi = 1, \ldots, k$; from this array we can compute the mean vector $\mathbf{z}$ and the covariance matrix $\mathbf{C}$. Element c_{ii} of $\mathbf{C}$ is the variance of x_i, the ith component of the $\mathbf{x}$ vectors, while element c_{ij} is the covariance between elements x_i and x_j of these vectors. This way, if elements x_i and x_j are uncorrelated, then $c_{ij} = c_{ji} = 0$.

Given that the $n \times n$ matrix $\mathbf{C}$ is real and symmetric, finding a set of n orthonormal eigenvectors always is possible.[11,20] Let $\mathbf{e}^i$ and λ_i for $i = 1, \ldots, n$ be the eigenvectors and corresponding eigenvalues of $\mathbf{C}$ arranged in decreasing order. Let A be a transformation matrix whose rows are formed by the eigenvectors of $\mathbf{C}$ ordered decreasingly from their corresponding eigenvalue. Therefore, we define the *Hotelling transform* based on the transformation matrix A that is used to map the $\mathbf{x}$ vectors into corresponding $\mathbf{y}$ vectors, according to the expresion,

$$\mathbf{y} = A(\mathbf{x} - \mathbf{z}). \tag{1}$$

An important result from this transformation is that the covariance matrix computed from the $\mathbf{y}$ vectors is a diagonal matrix whose off-diagonal elements are 0, in other words, the elements of the $\mathbf{y}$ vectors are uncorrelated. Additionally, Eq. (1) establishes a new coordinate system whose origin is at the coordinates of $\mathbf{z}$ and whose axes point in the direction of maximum variance; in the case of multispectral images, the corresponding principal components obtained from the Hotelling transform have the characteristic that the highest contrast is contained in the first two components (about 94% of the total variance).

2.2 K-means clustering

This classification algorithm is used to identify clusters from n-dimensional data points (also considered as vectors). The mathematical treatment of the algorithm is briefly described as follows. Given a set of data $\{\mathbf{x}^1, \ldots, \mathbf{x}^Q\}$ consisting in Q observations from a random sample $X \in \mathbb{R}^n$, the method searches to subdivide the data set into K clusters. Particularly, a cluster is conformed by a set of data whose interdistances with points of the same cluster are smaller than the distances with points outside the cluster. The $\mathbf{p}^\xi$ vectors, for $\xi = 1, \ldots, K$ represent the centers of such groups. Therefore, the purpose of the algorithm is to determine these vectors, as well as to assign the data points to some cluster such that the sum of the square distance of each point to its closer $\mathbf{p}^\xi$ vector be a minimum.[2]

Mathematically, for each point $\mathbf{x}^q$, with $q = 1, \ldots, Q$, let $d_{q,\xi} \in \{0, 1\}$ be a set of binary variables indicating which of the K clusters the point $\mathbf{x}^q$ should be assigned, such that if the point is assigned to the ξ cluster, then $d_{q,\xi} = 1$ and $d_{q,j} = 0$ for $j \neq \xi$. The following objective function is defined such that

$$J = \sum_{q=1}^{Q} \sum_{\xi=1}^{K} d_{q,\xi} \|\mathbf{x}^q - \mathbf{p}^\xi\|^2, \tag{2}$$

which represents the sum of the square distances between each point to its assigned $\mathbf{p}^\xi$ vector. Because this function has the objective of finding values of $d_{q,\xi}$ and $\mathbf{p}^\xi$ that minimize J, the algorithm performs an iterative process that involves two optimization stages at each iteration. First, initial values for $\mathbf{p}^\xi$ are chosen, then the algorithm minimizes J with respect to $d_{q,\xi}$ with a fixed $\mathbf{p}^\xi$. In the second step, the algorithm minimizes J with respect to $\mathbf{p}^\xi$ maintaining $d_{q,\xi}$ fixed. This two optimization steps are repeated until convergence. At the end of the procedure all the points are classified as members of some of the K clusters.

3. LATTICE ASSOCIATIVE MEMORIES FOR IMAGE CLASSIFICATION

The technique that will be presented in this section has emerged from hyperspectral image analysis, whose results have shown to be an efficient method for the determination of constituent materials spectra,[25,26,31] as well as an important tool for pigments extraction.[30] This section introduces the basic lattice concepts and mathematical operations needed to understand the proposed classification method and the case study presented in Section 4. The first subsection provides background related to lattice matrix algebra operations, while the second subsection introduces lattice associative memories as the fundamental tool for the method here discussed.

3.1 Lattice matrix algebra

Lattice algebra based operations, in which the usual matrix operations of addition and multiplication are replaced by corresponding lattice operations, have found increasing applications, such as pattern recognition,[22] associative memories in image processing,[23,24,28] computational intelligence,[9] industrial applications modeling and knowledge representation,[13] and hyperspectral image segmentation.[10,25,26,29] In the following lines we introduce the foundations of these operations.

The maximum or minimum of two numbers usually denoted as $\max(x, y)$ and $\min(x, y)$, will be written as binary operators using the "join" and "meet" symbols employed in lattice theory,[1] i.e., $x \vee y = \max(x, y)$ and $x \wedge y = \min(x, y)$. For example, the maximum of two matrices X, Y of the same size $m \times n$ is defined as $(X \vee Y)_{ij} = x_{ij} \vee y_{ij}$, for all $i = 1, \ldots, m$ and $j = 1, \ldots, n$. Inequalities between matrices are also verified elementwise, e. g., $X \leq Y$ if and only if $x_{ij} \leq y_{ij}$. Furthermore, the *conjugate matrix* X^* is defined as $-X^T$ where X^T denotes usual matrix transposition, or equivalently, $(X^*)_{ij} = -x_{ji}$, hence $X \vee Y = (X^* \wedge Y^*)^*$. Two important operations are the *max-sum* of appropriately sized matrices X, Y and the *min-sum* of X, Y defined, respectively, for all $i = 1, \ldots, m$ and $j = 1, \ldots, n$, as follows:

$$(X \boxtimes Y)_{ij} = \bigvee_{k=1}^{p} (x_{ik} + y_{kj}) \quad \text{and} \quad (X \boxtimes Y)_{ij} = \bigwedge_{k=1}^{p} (x_{ik} + y_{kj}) \,. \tag{3}$$

The relationship $(X \boxtimes Y)^* = Y^* \boxtimes X^*$ holds for X, Y, and establishes the *duality* between both types of lattice matrix sums. For $p = 1$ we have $\mathbf{y} \boxtimes \mathbf{x}^T = \mathbf{y} \boxtimes \mathbf{x}^T$, thus these lattice operations reduce to the *outer sum* of two vectors $\mathbf{x} \in \mathbb{R}^n$ and $\mathbf{y} \in \mathbb{R}^m$, defined by the $m \times n$ matrix

$$\mathbf{y} \oplus \mathbf{x}^T = \begin{pmatrix} y_1 + x_1 & \cdots & y_1 + x_n \\ \vdots & \ddots & \vdots \\ y_m + x_1 & \cdots & y_m + x_n \end{pmatrix}. \tag{4}$$

3.2 Lattice associative memories

Lattice based operations have been applied for pattern recognition problems as the computational model for a novel class of neural networks that are used as associative memories.[22,24] Let $(\mathbf{x}^1, \mathbf{y}^1), \ldots, (\mathbf{x}^k, \mathbf{y}^k)$ be k vector pairs with $\mathbf{x}^\xi = (x_1^\xi, \ldots, x_n^\xi)^T \in \mathbb{R}^n$ and $\mathbf{y}^\xi = (y_1^\xi, \ldots, y_m^\xi)^T \in \mathbb{R}^m$ for $\xi = 1, \ldots, k$. Given a set of vector associations $\{(\mathbf{x}^\xi, \mathbf{y}^\xi) \ : \ \xi \in k\}$ we introduce a pair of associated matrices (X, Y), where $X = (\mathbf{x}^1, \ldots, \mathbf{x}^k)$ and $Y = (\mathbf{y}^1, \ldots, \mathbf{y}^k)$, with an association given by $(\mathbf{x}^\xi, \mathbf{y}^\xi)$ for $\xi \in k$. Thus, X is of dimension $n \times k$ with i, jth entry x_i^j and Y is of dimension $m \times k$ with i, jth entry y_i^j. Two $m \times n$ *lattice associative memories* able to store k vectors such that, for $\xi = 1, \ldots, k$, the memory recalls $\mathbf{y}^\xi$ when is presented the vector $\mathbf{x}^\xi$ are defined as follows. The *min-memory* W_{XY} and the *max-memory* M_{XY}, both of size $m \times n$, that store a set of associations (X, Y) are given by the expressions

$$W_{XY} = \bigwedge_{\xi=1}^{k} [\mathbf{y}^\xi \oplus (-\mathbf{x}^\xi)^T] \qquad ; \qquad w_{ij} = \bigwedge_{\xi=1}^{k} (y_i^\xi - x_j^\xi), \tag{5}$$

$$M_{XY} = \bigvee_{\xi=1}^{k} [\mathbf{y}^\xi \oplus (-\mathbf{x}^\xi)^T] \qquad ; \qquad m_{ij} = \bigvee_{\xi=1}^{k} (y_i^\xi - x_j^\xi). \tag{6}$$

The left part of Eqs. (5) and (6) are in matrix form, while the expressions to the right correspond to the i, jth entry of *min-W* and *max-M* memories, respectively. In this case the memories are named *lattice hetero-associative* memories (LHAMs); we speak of a *lattice auto-associative* memory (LAAM) if $X = Y$; hence, $X \boxtimes X^* = (X^*)^* \boxtimes X^* = (X \boxtimes X^*)^*$, then $M = W^*$. Hence, the *min-* and *max*-memories are dual to each other in the sense of matrix conjugation and $m_{ij} = -w_{ji}$.

3.3 Classification procedure from LAAMS

The classification method here discussed is based on the assumption that many of the spectral pixels registered in a multispectral scene are conformed by spectral mixtures of the constituent materials spectra, at different proportions, mathematically,

$$\mathbf{x} = \sum_{i=1}^{K} a_i \mathbf{s}^i + \mathbf{r} = S\mathbf{a} + \mathbf{r} \tag{7}$$

$$a_i \geq 0 \ \forall i \quad \text{and} \quad \sum_{i=1}^{K} a_i = 1, \tag{8}$$

where $\mathbf{x} \in \mathbb{R}^n$ is a spectral pixel acquired over n bands, $S = \{\mathbf{s}^1, \ldots, \mathbf{s}^K\}$ is a matrix whose columns are the spectra of constituent materials (also known as *endmembers*), $\mathbf{a}$=$(a_1, \ldots, a_K)^T$ is a K-dimensional vector of corresponding fractional abundances present in $\mathbf{x}$ and $\mathbf{r}$ is a noise vector.[14] This model represents a minimum convex set or *simplex* enclosing most of the spectral data, where the K pure pixels spectra are the vertices of the corresponding simplex.

The matrix memories W_{XX} and M_{XX}, computed from a given set of vectors $X = \{\mathbf{x}^1, \ldots, \mathbf{x}^k\} \in \mathbb{R}^n$, are able to derive an n-dimensional simplex enclosing most if not all of the vectors in the given space. These points will correspond to the vertices of the n-simplex and can be extracted from the columns of W and M. As it was shown in,[25,30] for multispectral and hyperspectral data sets these vertices represent the "purest" spectral pixels

or constituent materials spectra that can be used for classification. In addition, given that the column values of LAAMs are not directly related with the set of original data X (for example W usually has negative values by definition), an *additive scaling* is required to relate the column values with X. Thus, two scaled matrices, denoted respectively as $\overline{W}$ and $\overline{M}$, are defined for all $i = 1, \ldots, n$ according to the following expressions,

$$\overline{\mathbf{w}}^{\,i} = \mathbf{w}^i + \bigvee_{\xi=1}^{k} x_i^{\xi} \qquad ; \qquad \overline{\mathbf{m}}^{\,i} = \mathbf{m}^i + \bigwedge_{\xi=1}^{k} x_i^{\xi}, \tag{9}$$

where $\mathbf{u} = \vee_{\xi=1}^{k} \mathbf{x}^{\xi}$ and $\mathbf{v} = \wedge_{\xi=1}^{k} \mathbf{x}^{\xi}$ denotes, respectively, the *maximum* and *minimum vector bounds* of X, and whose entries are defined for all $i = 1, \ldots, n$. Once the columns of $\overline{W}$ and $\overline{M}$ have been scaled, a fundamental result from this method is that the set of points $\overline{M} \cup \overline{W} \cup \{\mathbf{u}, \mathbf{v}\}$, forms a *convex polytope* $\mathfrak{B}$ with $2(n+1)$ vertices that contains X. For classification purposes, a subset $\mathcal{C}$ of $\{\overline{W} \cup \mathbf{u} \cup \overline{M} \cup \mathbf{v}\}$ should be considered. As a first approximation it is possible to select a number of $\sqrt{n}$ columns to classify the data. In practice, however, the election of this subset will depend on the number of materials to be classified. In order to determine which columns should be consider for classification, an election based on the matrix of correlation coefficients provides the most representative spectral vectors in the image. Finally, once the subset $\mathcal{C}$ has been determined, it is possible to estimate the fractional abundances of each constituent material for all the vectors in the n-dimensional data.

The estimation of fractional abundances, known as *spectral unmixing*, can be performed through the inversion of Eq. (7) subject to the imposed restrictions specified by Eq. (8). In the unconstrained case, a simple solution can be obtained through the least square estimation method, expressed by,

$$\mathbf{a} = S^{+}\mathbf{x} = (S^T S)^{-1} S^T \mathbf{x}, \tag{10}$$

where S^{+} denotes the Moore-Penrose pseudoinverse matrix. However, for practical applications requiring that the $\mathbf{a}$ coefficients satisfy the non-negativity condition, relaxing the full additivity, the *non negative least square* numerical method (NNLS)[16] may be used as a good approximation. Finally, the spectral classification can be performed according to the computed fractional abundances.

4. SIMULATION RESULTS

The previously introduced techniques have been evaluated using two multispectral data sets registered by the CAVE Project,[33] which are available for research purposes. The scenes were captured using a CIE standard illuminant D65, a cooled CCD camera, and VariSpec liquid crystal tunable filters. Each image has a spatial resolution of 512×512 pixels, covering a spectral range from 400 nm to 700 nm at steps of 10 nm, and whose pixel values correspond to reflectance quantities. The data sets employed for our simulations are subimages of size 399×187 pixels that are conformed by two peppers similar in appearance, but one being real and the other being fake. Figures 1 and 2 present both subimages and the corresponding spectral curves obtained from each one of the peppers to highlight their spectral differences. It is clear that the spectral curves show significant differences for each case.

4.1 Application examples

Red peppers image

According to the authors the red pepper that appears in the upper part of the image is a real one, while the other is fake. Also, including the background and the bright parts spectra, the number of classes for the clustering process was set to four. Principal component analysis was first performed according to Eq. (1) computed from the 31 spectral bands of the image. From the total number of components produced by the transformation, we selected the first three components (C1, C2, C3) to produce a false color image; specifically, C1, C2, and C3 were used as the R, G, and B channels to produce a color image. Table 1, first row, displays the largest eigenvalues corresponding to components 1 to 9. On the other hand, the K-means clustering was realized according to the

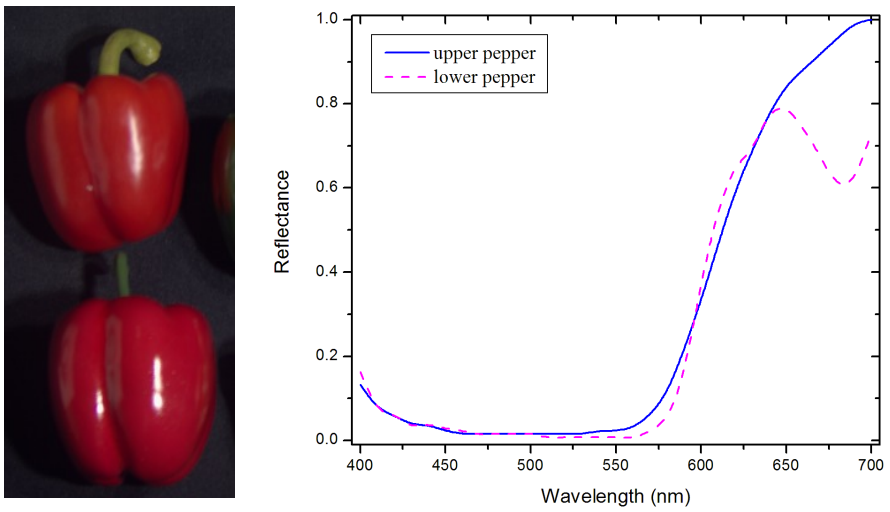

Figure 1. From left to right: first exemplar image conformed by two red peppers similar in appearance; corresponding spectral reflectance curves obtained from pixels [105,86] and [302,106], respectively.

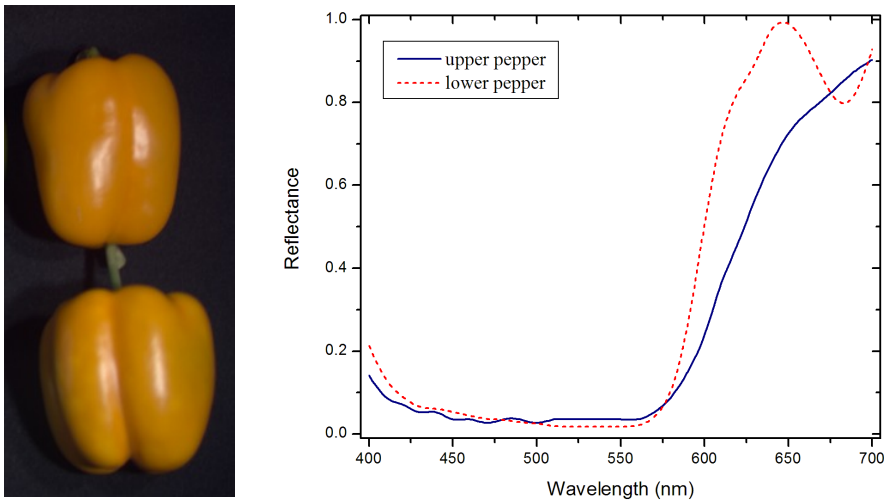

Figure 2. From left to right: second exemplar image conformed by two yellow peppers similar in appearance; corresponding spectral reflectance curves obtained from pixels [96,68] and [338,117], respectively.

Euclidian distance and the clustering process was repeated six times. Columns 2 and 3 of Figure 3 show the classification results obtained with both methods.

The use of LAAMs for multispectral image classification was realized as follows. Being X the matrix conformed by all the spectral vectors in the image, such that $X = (\mathbf{x}^1, \ldots, \mathbf{x}^k) \in \mathbb{R}^{31}$, with $k = 74613$, we computed W_{XX} and M_{XX} by means of Eqs. (5) and (6), respectively. The resulting scaled memories $\overline{W}$ and $\overline{M}$, both of size 31×31, were used to choose a reduced set of column vectors. As it was stated in,[25,26] contiguous columns are highly correlated being necessary to use some techniques to select a subset of them. A practical solution consisting of a matrix of linear correlation coefficients computed from each scaled memory, followed by a threshold

Table 1. Eigenvalues λ_i, for $i = 1, \ldots, 9$, computed with principal component analysis for both subimages.

IMAGE	λ_1	λ_2	λ_3	λ_4	λ_5	λ_6	λ_7	λ_8	λ_9
Red peppers	12541	1549	192	54	32	6	5	3	1
Yellow peppers	17371	384	31	12	7	2	2	1	1

process produces a subset of spectral vectors with low correlation coefficients.[26] For this exemplar image, from the 62 column vectors derived from $\overline{W} \cup \overline{M}$ a final selection of uncorrelated columns from a threshold value of 0.3 provided a reduced set containing 4 spectral vectors; thus, $\mathcal{C} = \{\overline{\mathbf{w}}^3, \overline{\mathbf{w}}^{14}, \overline{\mathbf{w}}^{15}, \overline{\mathbf{m}}^{17}\}$. Therefore, these column vectors conformed the columns of the S matrix in Eq.(7) and fractional abundances were estimated with the NNLS numerical method. Fourth column of Figure 3 shows the distribution of these spectral vectors along the image.

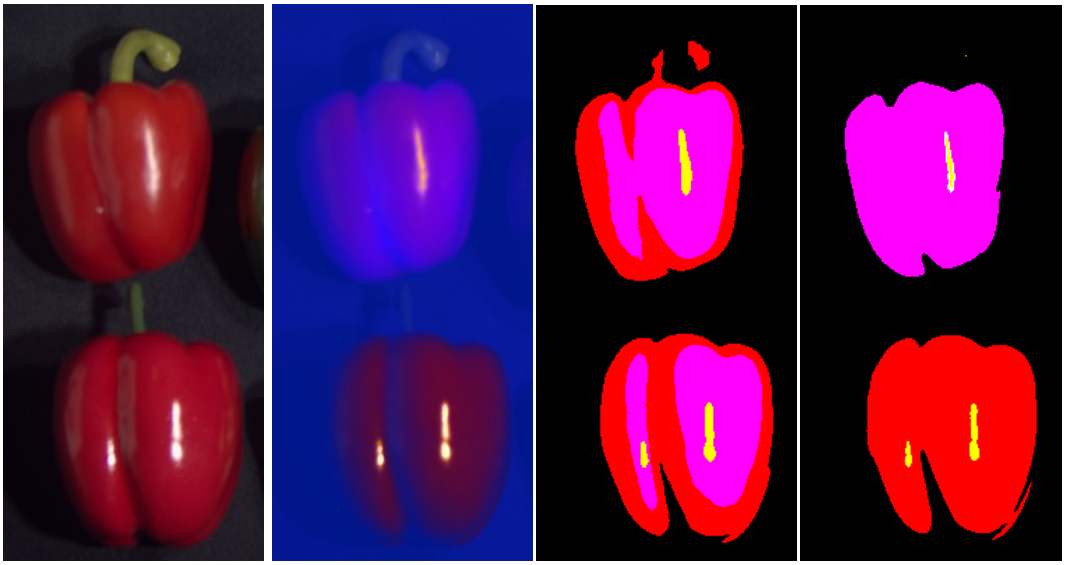

Figure 3. 1st column: color RGB image; 2nd column: false color image produced by the first components of PCA; 3rd column: classification produced by K-means clustering; 4th column: distribution of spectrally different classes obtained with the LAAMs method.

Yellow peppers image

For this exemplar image the upper pepper is real, while the lower one is fake. Hence, any of the previously discussed techniques should be able to classify these objects as members of two different classes. Firts, principal component analysis was applied to the 31 spectral bands of the image. From the total number of components the first three components were combined to produce a false color image. Table 1 presents the largest eigenvalues corresponding to components 1 to 9. Also, for the K-means clustering the number of classes to subdivide the image was set to four. The use of the Euclidian distance as distance metric and repeating the clustering 6 times produced the results shown in the third column of Figure 4.

The method based on LAAMs was applied to the data set X, conformed by all the spectral vectors in the image. From this set we computed W_{XX} and M_{XX} and their corresponding scaled versions $\overline{W}$ and $\overline{M}$. In order to select a reduced number of uncorrelated columns, a matrix of linear correlation coefficients was computed from each scaled memory. By selecting the column vectors with correlation coefficients less than 0.39 produced a reduced set containing 4 spectral vectors; thus, $\mathcal{C} = \{\overline{\mathbf{w}}^8, \overline{\mathbf{m}}^4, \overline{\mathbf{m}}^7, \overline{\mathbf{m}}^{17}\}$. The NNLS numerical method provided the fractional abundances for each one of these spectra at each pixel of the image. Figure 4, fourth column, displays the distribution of these spectral vectors along the image.

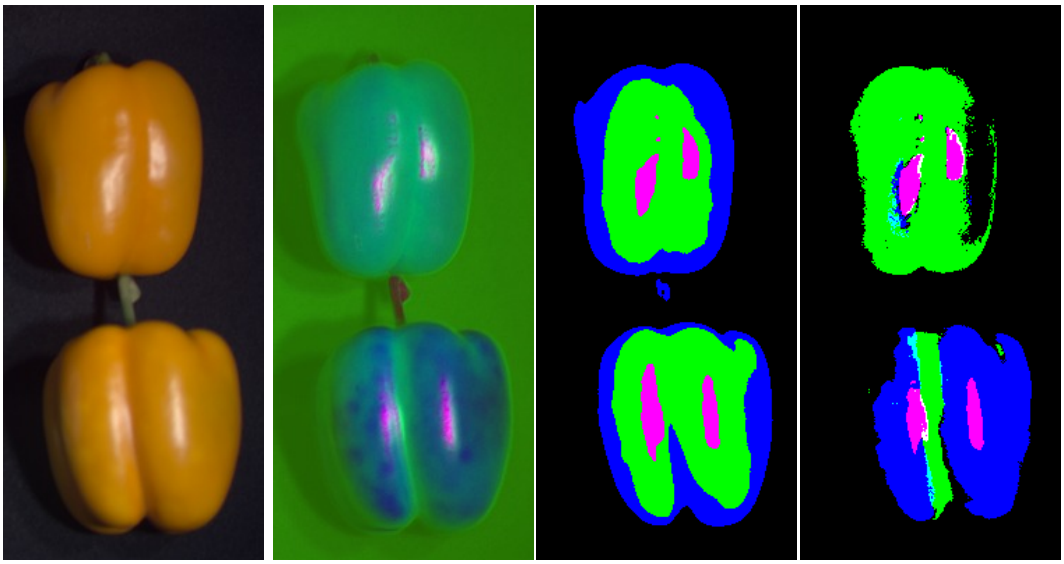

Figure 4. 1st column: color RGB image; 2nd column: false color image produced by the first components of PCA; 3rd column: classification produced by K-means clustering; 4th column: distribution of spectrally different classes obtained with the LAAMs method.

4.2 Comparison of results

According to the classification results shown in Figures 3 and 4, we can state that the LAAMs method and PCA produced the best results. For the first exemplar image, lattice auto-associative memories approximated the spectral curves of both real and fake peppers, which were used to classify the areas with similar spectra along the image; the pseudo color image corresponding to the forth column of Figure 3 allows a clear differentiation among the classes. Also, the false color image produced by the first components of PCA emphasizes the areas with different spectral reflectance. On the other hand, K-means clustering is able to classify correctly the spectra belonging to background and the bright areas; however, it classifies both peppers as members of the same class, which is not true. For the second exemplar image, both techniques PCA and the LAAMs method are able to differentiate between both peppers. This last, however, does not classify completely the upper pepper. The results obtained by K-means clustering are similar to the previous case. Therefore, the fact that the spectral curves of real and fake peppers present some similarities causes that the distances computed with K-means do not present large differences to discriminate between the two objects.

5. CONCLUSIONS

In this manuscript we have presented a review of three methods that can be used for materials classification from multispectral data. Beginning with the mathematical treatment of two well known methods, such as principal component analysis and K-means, we also have discussed the application of a novel technique, based on lattice auto-associative memories, for multispectral image classification. This technique is able to determine a minimum convex set enclosing most of the spectral data X by computing two lattice matrix memories, $\overline{W}$ and $\overline{M}$, respectively. Also, the points defining the convex set correspond to the "purest" spectral pixels or, alternatively, the spectra of materials conforming the scene. Hence, a reduced set of uncorrelated columns obtained from $\overline{W}$ or $\overline{M}$ can be employed for the spectral unmixing procedure. The application examples selected for our simulations present additional complexity because the objects are similar in appearance, but with some differences in their spectral curves. According to the classification results, the first three components computed from principal component analysis can be used to highlight areas with different spectral characteristics. Moreover, the use of $\overline{W}$ and $\overline{M}$ has provided good results for materials classification even in those cases with similar spectral curves. On the other hand, the classification produced by K-means clustering did not give good results because of similarities in the spectral curves of real and fake peppers, which causes that the distances computed by the algorithm are not

large enough to discriminate between them. In fact, for applications related to quality monitoring or materials classification, PCA and LAAMs are suitable techniques.

ACKNOWLEDGMENTS

The authors are grateful with the Cave Project for providing the multispectral images used for our simulations. Gonzalo Urcid thanks the National System of Research (Sni-Conacyt) for partial support through grant # 22036.

REFERENCES

1. Birkhoff, G. [Lattice Theory], 3rd ed, American Mathematical Society, Providence RI, (1967).
2. Bishop, C.M. [Pattern Recognition and Machine Learning], Springer, pp. 424–425, (2006).
3. Boardman, J.W. "Analysis, understanding and visualization of hyperspectral data as convex sets in n-space," Proc. of SPIE: Imaging Spectrometry, Vol. 2480, pp. 14–22, (1995).
4. Casini, A. Lotti, F. Picollo, M. Stefani L. and Buzzegoli, E. "Image spectroscopy mapping technique for non-invasive analysis of paintings," Studies in Conservation, Vol. 44, No. 1, pp. 39-48, (1999).
5. Easton, R.L. Knox, K.T. and Christens-Barry, W.A. "Multispectral imaging of the Archimedes Palimpsest," Proc. 32nd Annual Conference on Applied Imagery Pattern Recognition, pp. 111-118, (2003).
6. Easton R.L. and Knox, K.T. "Digital restoration of erased and damaged manuscripts," Proc. 39th Annual Convention of the Association of Jewish Libraries, pp. 1–8, (2004).
7. Farrand W.H., "Hyperspectral remote sensing of land and the atmosphere." In [Encyclopedia of Modern Optics], Vol. 1, Robert Guenther ed., pp. 395–403, (2005).
8. Fisher, C. Kakoulli, I. "Multispectral and hyperspectral imaging technologies in conservation: current research and potential applications," Reviews in Conservation, No. 7, pp. 3–16, (2006).
9. Graña, M. "A brief review of lattice computing," Proceedings of IEEE: World Congress on Computational Intelligence, pp. 1777–1781, Hong Kong, (2008).
10. Graña, M. Villaverde, I. Maldonado, J.O. Hernández, C. "Two lattice computing approaches for the unsupervised segmentation of hyperspectral images," Neurocomputing, Vol. 72, No. 10-12, pp. 2111–2120, (2009).
11. Gonzalez, R.C. Woods, R.E. [Digital Image Processing], 3rd edition, Pearson Education, (2008).
12. Hahn, F. "AE - Automation and Emerging Technologies: Multi-spectral Prediction of Unripe Tomatoes," Biosystems Engineering, Vol. 81, Issue 2, pp. 147–155, (2002).
13. Kaburlasos V.G. and Ritter G.X. (eds.), [Computational Intelligence based on Lattice Theory], Vol. 67. Springer Verlag, Heidelberg, Germany, (2007).
14. Keshava, N. "A survey of spectral unmixing algorithms," Lincoln Laboratory Journal, Vol. 14, No. 1, 55–78, (2003).
15. Kim, M.S. Lefcourt, A.M. Chen, Y. Tao, Y. "Automated detection of fecal contamination of apples based on multispectral fluorescence image fusion," Journal of Food Engineering, pp. 85– 91, (2005).
16. Lawson, C.L. Hanson, R.J. [Solving least squares problems], chap. 23, Prentice-Hall, Englewood Cliffs NJ, (1974).
17. Lettner M. and Sablatnig, R. "Multispectral imaging for analyzing ancient manuscripts," Proc. 17th European Signal Processing Conference, pp.1200-1204, Glasgow, Scotland, (2009).
18. Nascimento, J.M.P. Bioucas-Dias, J.M. "Vertex component analysis: a fast algorithm to unmix hyperspectral data," IEEE Trans. on Geoscience and Remote Sensing, Vol. 43, No. 4, pp. 898–910, (2005).
19. Nguyena, D.V. Rockeb, D.M. " On partial least squares dimension reduction for microarray-based classification: a simulation study," Vol. 46, No. 3, pp. 407–425, (2004).
20. Noble, B. Daniel, J.W. [Applied Linear Algebra], Pearson Education, (1988).
21. Park B., Windham W.R., Lawrence K.C., Smith D.P., "Contaminant classification of poultry hyperspectral imagery using a spectral angle mapper algorithm," Biosystems Engineering, Vol. 96, No. 3, pp. 323–333, (2007).

22. Ritter, G.X. Sussner, P. Díaz de León, J.L. "Morphological associative memories," IEEE Trans. Neural Networks, Vol. 9, No. 2, pp. 281–293, (1998).
23. Ritter, G.X. Urcid, G. and Iancu, L. "Reconstruction of noisy patterns using morphological associative memories," Journal of Mathematical Imaging and Vision, Vol. 19, No. 5, pp. 95–111, (2003).
24. Ritter, G.X. Gader, P. "Fixed Points of Lattice Transforms and Lattice Associative Memories." In [Advances in Imaging and Electron Physics], Vol. 144, P. Hawkes (ed.), Elsevier, San Diego CA, pp. 165–242, (2006).
25. Ritter, G.X. Urcid, G. Schmalz, M.S. "Autonomous single-pass endmember approximation using lattice auto-associative memories," Neurocomputing, Vol. 72, No. 10-12, pp. 2101–2110, (2009).
26. Ritter,G.X. Urcid, G. "Lattice algebra approach to endmember determination in hyperspectral imagery." In: [Advances in Imaging and Electron Physics], Peter W. Hawkes editor, Vol. 160, pp. 113-169, Elsevier, (2010).
27. Urcid, G. Valdiviezo-N., J.C. "Generation of lattice independent vector sets for pattern recognition applications," SPIE Proceedings: Mathematics of Data/Image Pattern Recognition, Compression, Coding, and Encryption X with Applications, Vol. 6700, pp. 67000C:1–12, (2007).
28. Urcid, G. Valdiviezo, J.C. Ritter, G.X. "Lattice algebra approach to color image segmentation," Journal of Mathematical Imaging and Vision, Vol. 42, No.2-3, pp. 150-162, (2012).
29. Valdiviezo, J.C. and Urcid, G. "Hyperspectral endmember detection based on strong lattice independence," Proc. SPIE: Applications of Digital Image Processing XXX, Vol. 6696, pp. 1–12, San Diego, CA, USA, (2007).
30. Valdiviezo, J.C. and Urcid, G. "Multispectral images segmentation of ancient documents with lattice memories," OSA Proc.: Digital Image Processing and Analysis, Tucson, AZ, (2010).
31. Valdiviezo, J.C. Urcid, G. "Convex set approaches for material quantification in hyperspectral imagery." In: [Earth Observation], Rustam B. Rustamov and Saida E. Salahova eds. (2012).
32. Yamaguchi, M. Teraji, T. Ohsawa, K. Uchiyama, T. Motomura, H. Murakami, Y. Ohyama, N. "Color image reproduction based on the multispectral and multiprimary imaging: experimental evaluation," Proc. SPIE, Vol. 4663, No. 15 (2002).
33. Yasuma, F. Mitsunaga, T. Iso, D. and Nayar, S.K. "Generalized assorted pixel camera: post-capture control of resolution, dynamic range and spectrum," Technical Report, Department of Computer Science, Columbia University CUCS-061-08, Nov, (2008).
34. Zhengrong, L. MacFall, J.R. Harrington, D.P. "Parameter estimation and tissue segmentation from multispectral MR images," IEEE Trans. on Medical Imaging, Vol. 13, No. 3, pp. 441–449, (1994).